Earth and Space Science

RESEARCH ARTICLE
10.1029/2021EA002030

Analysis of Relationships Between ENSO Events and Atmospheric Angular Momentum Variations

Nan Yu[1,2], Huanling Liu[3,4], Gang Chen[1], Wei Chen[5], Jim Ray[6], Hanjiang Wen[3], and Nengfang Chao[1]

[1]College of Marine Science and Technology, China University of Geosciences, Wuhan, China, [2]Hubei Key Laboratory of Marine Geological Resources, China University of Geosciences, Wuhan, China, [3]Chinese Academy of Surveying and Mapping, Beijing, China, [4]Key Laboratory of Earth Observation and Geospatial Information Science, Beijing, China, [5]School of Geodesy and Geomatics, Wuhan University, Wuhan, China, [6]National Oceanic and Atmospheric Administration, Silver Spring, MD, USA

Abstract The El Niño–Southern Oscillation (ENSO) event has a long incubation process, during which the interannual variation of length-of-day (LOD) and the atmospheric angular momentum (AAM) series will be quickly affected due to the interaction between sea and air. Based on the comparisons between filtered interannual LOD variation, the AAM, the Oceanic Niño Index (ONI), and the Southern Oscillation Index (SOI) for the period of January 1953 and December 2013, the relationships among them and ENSO are studied. The results demonstrate that AAM changes and SOI/ONI series have similar waveform structures and trends. Interannual LOD variations, atmospheric LOD excitations, and ENSO indices such as the SOI and ONI are well correlated as a consequence of angular momentum conservation. AAMs can be accurately modeled at present, taking ESMGFZ as an example, its sampling interval can reach 3 hr, and can realize accurate prediction in the next 90 days. Consequently, AAM series also can be used as an index for ENSO events and has its own advantages compared with SOI/ONI.

Key Points:

- The atmospheric angular momentum (AAM) changes and SOI/ONI series have similar waveform structures and trends
- Interannual atmospheric LOD excitations and SOI/ONI ENSO indices are well correlated as a consequence of angular momentum conservation
- By multiplying a gain factor of *k*, AAM series also can be used as an index for ENSO events

Correspondence to:
G. Chen,
ddwhcg@cug.edu.cn

Citation:
Yu, N., Liu, H., Chen, G., Chen, W., Ray, J., Wen, H., & Chao, N. (2021). Analysis of relationships between ENSO events and atmospheric angular momentum variations. *Earth and Space Science*, *8*, e2021EA002030. https://doi.org/10.1029/2021EA002030

Received 18 SEP 2021
Accepted 4 NOV 2021

Author Contributions:
Conceptualization: Nan Yu
Formal analysis: Nan Yu, Gang Chen
Methodology: Nan Yu, Jim Ray
Software: Nengfang Chao
Supervision: Huanling Liu, Hanjiang Wen
Validation: Nan Yu, Wei Chen
Writing – original draft: Nan Yu
Writing – review & editing: Jim Ray

1. Introduction

El Niño and the Southern Oscillation, also known as ENSO, is a periodic fluctuation in sea surface temperature (SST; El Niño) and the air pressure of the overlying atmosphere (Southern Oscillation) across the equatorial Pacific Ocean. ENSO is the most prominent interannual climate variability on Earth with large ecological and societal impacts (e.g., Mcphaden et al., 2006; Rasmusson & Wallace, 1983; Ropelewski & Halpert, 1985; Trenberth & Hoar, 1997; Xin et al., 2016; Zhang et al., 2015). Although the exact initiating causes of an ENSO warm or cool event are not fully understood, the two components of ENSO—atmospheric pressure and SST—are known to be strongly related.

The Southern Oscillation Index (SOI) is one conventional measure of the large-scale fluctuations in air pressure occurring between the western and eastern tropical Pacific during El Niño and La Niña episodes (e.g., Walker & Bliss, 1932). Traditionally, this index has been calculated based on the differences in air pressure anomaly between Tahiti and Darwin, Australia (e.g., Allan et al., 1991; Können et al., 1998). In general, smoothed time series of the SOI correspond very well with changes in ocean temperatures across the eastern tropical Pacific. The negative phase of the SOI represents below-normal air pressure at Tahiti and above-normal air pressure at Darwin. Prolonged periods of negative SOI values coincide with abnormally warm ocean waters across the eastern tropical Pacific typical of El Niño episodes. Prolonged periods of positive SOI values coincide with abnormally cold ocean waters across the eastern tropical Pacific typical of La Niña episodes (e.g., Power & Kociuba, 2011). Monitoring of ENSO conditions can also focus on SST anomalies in four geographic regions of the equatorial Pacific (refer to Table 1). SST anomalies equal to or greater than 0.5°C in the Niño 3.4 region (comprising portions of Niño regions 3 and 4, from 170°W to 120°W longitude) are indicative of ENSO warm phase (El Niño) conditions, while anomalies less than or equal to −0.5°C are associated with cool phase (La Niña) conditions. This standard of measure ENSO is known as the Oceanic Niño Index (ONI; e.g., Deliège & Nicolay, 2017; Wilson, 2010).

Changes in the excess length-of-day (LOD), compared to 86,400 SI s, reflect variations of the speed of the Earth's axial rotation. The nontidal LOD variations, which change on all observable time scales, from subdaily to decadal and longer, are related with the angular momentum exchange within the Earth system (e.g.,

Table 1
The NINO Regions (See Figure 2) Cover the Following Areas

	NINO 1	NINO 2	NINO 3	NINO 4	NINO 3.4
Area	5°–10°S, 80°–90°W	0°–5°S, 80°–90°W	5°N–5°S, 150°–90°W	5°N–5°S, 160°E–150°W	5°N–5°S, 120°–170°W

Brzeziński et al., 2002; Davies et al., 2014; Gross, 2015; Roberts & Aurnou, 2012; Yu et al., 2018, 2021). Interannual LOD variations have been less clear and have been characterized by signals with a wide range of periods and varying amplitudes, including a peak at about 5–6 years. This 5–6-year oscillation is only obvious in the residuals of the differences between geodetic and atmospheric LOD excitations, with an amplitude about 0.2–0.3 ms. Many studies discussed possible excitation mechanisms in the deep Earth for this 5–6-year oscillation and already obtained many useful conclusions (e.g., del Rio et al., 2000; Duan et al., 2018; Hao & Chao, 2018; Holme & De Viron, 2013; Liao & Greiner-Mai, 1999; Silva et al., 2012; Yu et al., 2020). Except for this 5–6-year oscillation, interannual LOD variations are also related with ENSO events. That is because the ENSO cycle has a long incubation process, during which the interannual LOD variations will be quickly affected by the interaction of the sea and the air (Chao, 1989; Dickey et al., 1994; Feissel & Gavoret, 2013; Liu et al., 2005; Pavlis et al., 2017).

We focus on the interannual (2–8 years) signals in atmosphere, LOD observation, and SOI/ONI series. By working in the time domain rather than the frequency domain, we compare interannual signals in geodetic LOD excitations from International Earth Rotation and Reference Systems Service (IERS) 14C04, atmospheric excitations from NCEP (National Centers for Environmental Prediction; e.g., Kalnay et al., 1996, and revised by Zhou et al. [2006]), and ESMGFZ (Earth System Modeling group at GFZ; e.g., Dobslaw & Dill, 2018) model AAM (atmospheric angular momentum) series, SOI, and ONI series from Australian Bureau of Meteorology. Sliding window average filtering is applied to both original IERS 14C04 geodetic, NCEP/ESMGFZ atmospheric excitation, and SOI/ONI series to remove their variations longer than decadal and those signals shorter than about 2 years. The scientific issues in our study contain two parts. First, why AAM series can be used as an index for ENSO events. By calculating the correlation coefficients between filtered interannual ONI, SOI, and NCEP excitation series, we find NCEP excitation series are highly correlated with both ONI and SOI series, which means that there are useful information of ENSO events in AAM series. Second, how AAM can be used as an index of ENSO events. Here, we derive a gain factor of k to make AAM series consistent with ONI and SOI series.

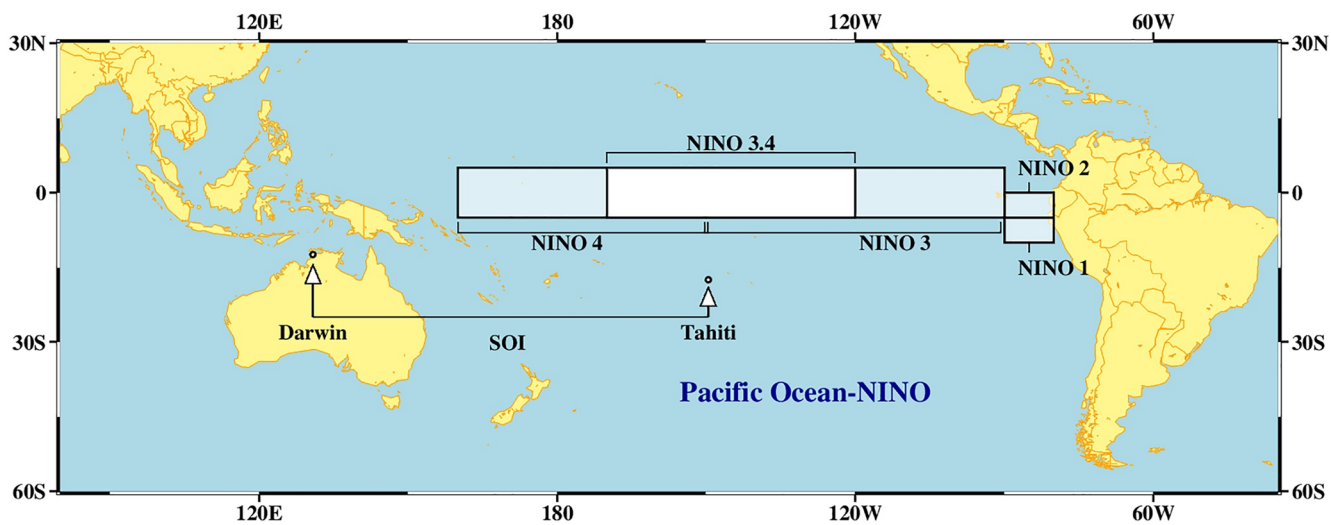

Figure 1. NINO regions.

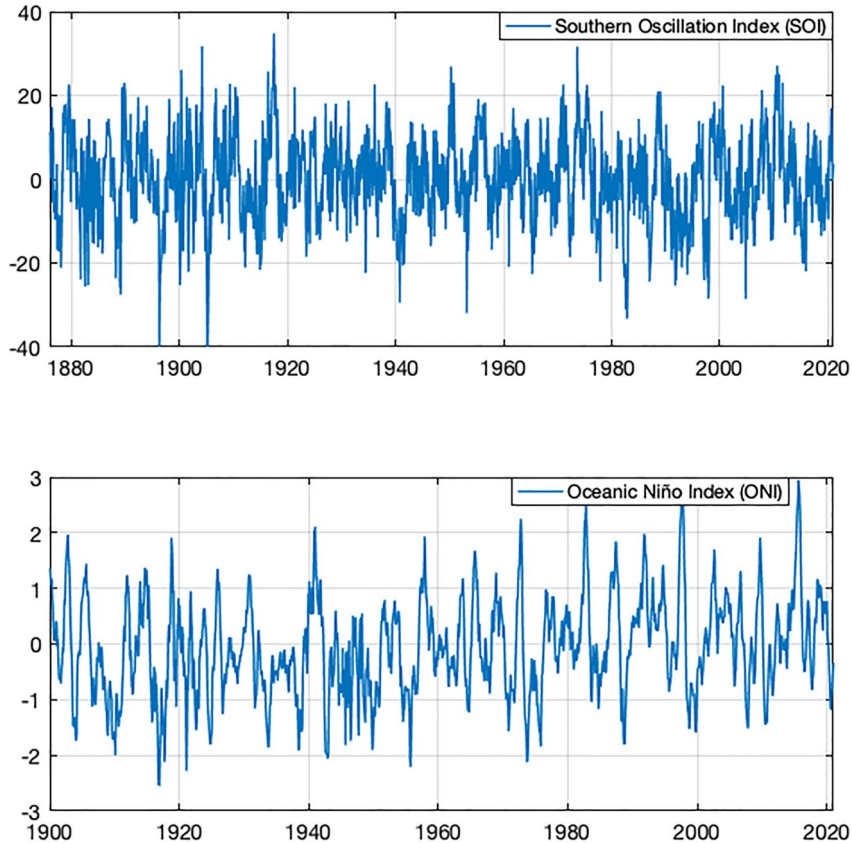

Figure 2. Southern Oscillation Index (SOI) series and Oceanic Niño Index (ONI) series provided by Australian Bureau of Meteorology.

2. Data

The SOI gives an indication of the development and intensity of El Niño or La Niña events in the Pacific Ocean. The SOI (no units) is calculated using the pressure differences between Tahiti and Darwin. Sustained negative values of the SOI lower than −7 often indicate El Niño episodes. These negative values are usually accompanied by sustained warming of the central and eastern tropical Pacific Ocean, a decrease in the strength of the Pacific

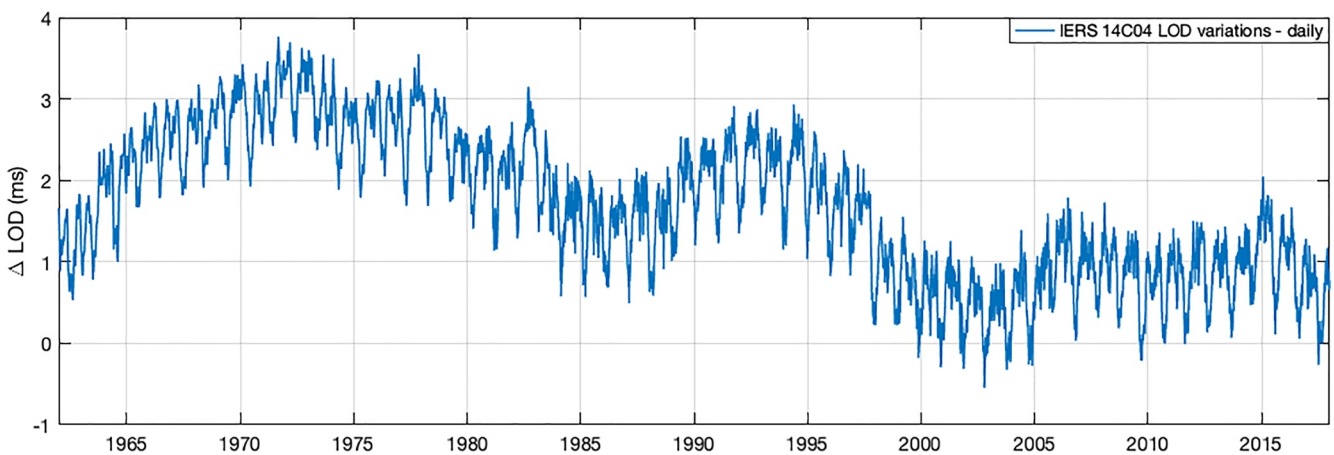

Figure 3. Length-of-day (LOD) variations calculated by International Earth Rotation and Reference Systems Service (IERS) 14C04. The unit of geodetic LOD excitations is ms.

Table 2
Tidal Constituents Estimated and Removed From AAM and OAM From ESMGFZ

Partial tide	Frequency (hr^{-1})
P_1	14.9589314
S_1	15.0000000
K_1	15.0410686
N_2	28.4397295
M_2	28.9841042
L_2	29.5284789
T_2	29.9589333
S_2	30.0000000
R_2	30.0410667
T_3	44.9589300
S_3	45.0000000
R_3	45.0410700

Trade Winds, and a reduction in winter and spring rainfall over much of eastern and northern Australia. Sustained positive values of the SOI greater than +7 are typical of a La Niña episode. They are associated with stronger Pacific trade winds and warmer sea temperatures to the north of Australia. Waters in the central and eastern tropical Pacific Ocean become cooler during this time. Together, these give an increased probability that eastern and northern Australia will be wetter than normal.

There are a few different methods for calculating the SOI. Here, we use the SOI data provided by Australian Bureau of Meteorology (http://www.bom.gov.au/climate/enso/soi_monthly.txt, see Figure 1). The method used by the Australian Bureau of Meteorology is the Troup SOI which is the standardized anomaly of the mean sea level pressure (MSLP) difference between Tahiti and Darwin.

$$\mathrm{SOI} = 10 \times \frac{\left(Pdiff - Pdiffav\right)}{\mathrm{SD}\left(Pdiff\right)} \tag{1}$$

where $Pdiff$ = average (Tahiti MSLP for the month) − average (Darwin MSLP for the month), $Pdiffav$ = long-term average of $Pdiff$ for the month in question, and $SD(Pdiff)$ = long-term standard deviation of $Pdiff$ for the month in question.

The multiplication by 10 is a convention. Using this convention, the SOI ranges from about −35 to about +35, and the value of the SOI can be quoted as a whole number. The SOI is usually computed on a monthly basis, with values over longer periods such as a year being sometimes used. Daily or weekly values of the SOI do not convey much in the way of useful information about the current state of the climate, and accordingly the Bureau of Meteorology does not issue them. Daily values in particular can fluctuate markedly because of daily weather patterns and should not be used for climate purposes.

During El Niño, SSTs in the central and eastern Pacific Ocean become warmer than average, while La Niña is characterized by cooler than average SSTs in the same regions. In order to monitor the Pacific Ocean for signs of El Niño or La Niña, climatologists use several SST indices. These indices simply refer to the difference from the long-term (1961–1990) mean of the SST in several regions located along the equatorial Pacific. These regions are called NINO 1 and NINO 2 (which lie on the South American coast), NINO 3 and NINO 3.4 (which occupy the eastern and central equatorial Pacific, respectively), and NINO 4 (located in the western Pacific). NINO 3.4 partially overlaps both the NINO 3 and NINO 4 regions, and measure of NINO 3.4 SST is taken as the standard called ONI. For monitoring of ENSO events, climatologists often cite sustained monthly ONI values above +0.5°C as typical of El Niño conditions, with values of below −0.5°C as that of La Niña.

Here, we use the ONI data provided by Australian Bureau of Meteorology as another evaluation criterion for ENSO events (http://www.bom.gov.au/climate/enso/nino34-monthly.txt).

The EOP 14C04 (IAU2000A version) series from the IERS provides internationally recognized EOP, recently updated to be consistent with the new ITRF2014 terrestrial reference frame (see hpiers.obspm.fr/eoppc for details). Past versions of this series, which is based on a nonrigorous combination of raw measurements made by independent space geodetic observing systems, have been most widely used for excitation studies (e.g., Altamimi et al., 2016; Bizouard et al., 2017). The tidal effects are removed with the model recommended by the IERS 2010

Table 3
Data Sets Used in This Study

	SOI	ONI	IERS 14C04	NCEP AAMs	ESMGFZ AAMs
Availability	Since 1876	Since 1900	Since 1962	Since 1948	Since 1976
Resolution	1 month	1 month	1 day	6 hr	3 hr

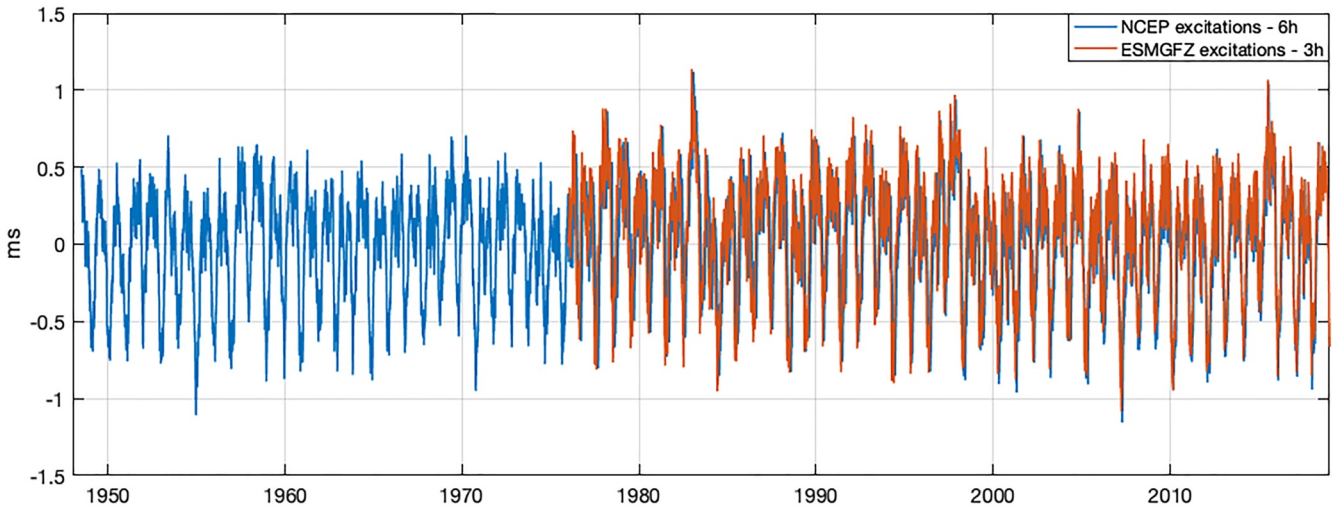

Figure 4. Geophysical LOD excitations from National Centers for Environmental Prediction (NCEP) and Earth System Modeling group at GFZ (ESMGFZ) atmospheric angular momentum (AAM) series. The unit of AAMs is ms.

conventions (e.g., Petit & Luzum, 2010; Figure 3). The Fortran routine RGZONT2.F provided by R. Gross (JPL) through the IERS website is applied here to derive this correction, which includes variations due to the elastic body tide (Yoder et al., 1981), the inelastic body tide (J. Wahr & Bergen, 1986), and the ocean tide (Kantha et al., 1998), see http://tai.bipm.org/iers/convupdt/convupdt_c8.html.

The portion caused by zonal tides of the solid Earth and oceans, which can exceed 1 ms peak-to-peak, is accurately known from geophysical models. The remaining nontidal LOD variations, over time scales shorter than about 2 years, reach a similar magnitude and are mainly seasonal and caused by the dynamic interaction of the solid Earth with its fluid envelopes (atmosphere, oceans, and continental hydrology). The dominant part of subbiennial LOD variations is attributable to the angular momentum carried by the zonal winds. LOD changes over longer spans are ultimately largest but involve unrelated processes in the deep Earth.

NCEP reanalysis products (e.g., Kalnay et al., 1996) span the period from 1948 to the present and were obtained from the IERS Special Bureau for the Atmosphere. The data set contains 6-hr values of AAM driven by changes in atmospheric pressure and atmospheric winds. The angular momentum due to winds has been computed as described in Zhou et al. (2006), who reprocessed AAM series by integrating zonal and meridional winds from the Earth's surface to 10 hPa, the top of the atmospheric model. The surface topography is taken into account when calculating the atmospheric motion term (e.g., Aoyama & Naito, 2000). The ESMGFZ routinely also provides EAMF (effective angular momentum functions) describing the nontidal geophysical excitations of Earth orientation changes due to mass redistribution and relative motion in atmosphere (e.g., Dobslaw & Dill, 2018). ESMGFZ AAM is based on reanalysis and operational analysis outputs from ECMWF (European Centre for Medium-Range Weather Forecasts). The ESMGFZ AAM temporal resolution is 3 hr (given at 0.5° equiangular grid points). Tidal variations for 12 most relevant frequencies are fitted and removed by ESMGFZ from the data to retain the nontidal signals only (see Table 2). Further information on the products is provided via the webpage www.gfz-potsdam.de/en/esmdata. Detailed information of the data sets used in this paper is listed in Table 3.

For the convenience of comparison with geodetic LOD excitations, NCEP/ESMGFZ AAMs are converted to geophysical LOD excitations first. The AAM series consist of two terms, usually referred to as the matter (or mass) and the motion terms (e.g., Lambeck, 1980; Munk & MacDonald, 1960; J. M. Wahr, 1982). The matter term describes the influence of mass redistribution on the Earth's inertia tensor, whereas the motion term corresponds to the relative angular momentum change with respect to the mean rotating reference system (e.g., Gross, 2015).

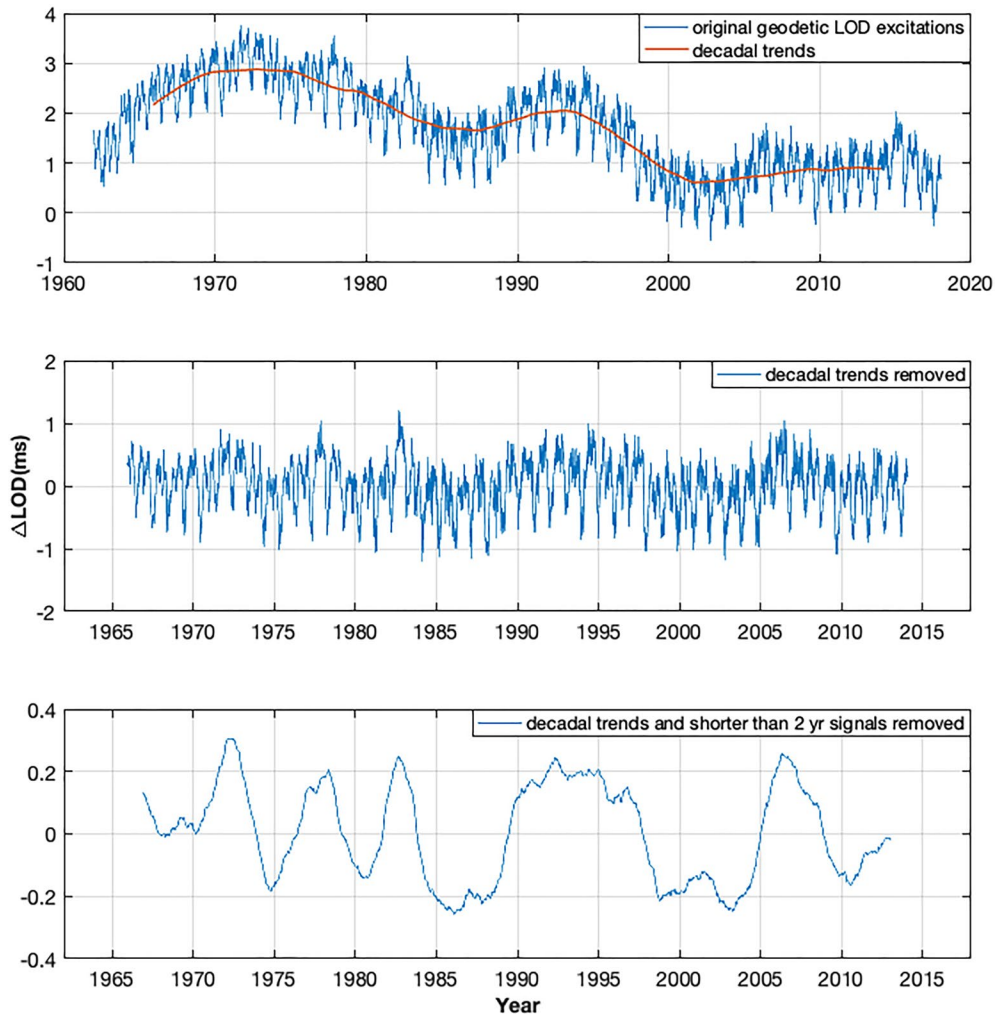

Figure 5. (top panel) Geodetic LOD excitations from IERS 14C04 over the recent period from January 1, 1962 till December 31, 2018. The blue color is the original geodetic LOD excitation series and the red color is the decadal trends determined by 8-year sliding window average filtering. (middle panel) Geodetic LOD excitations after decadal trends removed. (bottom panel) Interannual signals after removing both decadal trends and signals shorter than 2 years. The unit of geodetic LOD excitations is ms.

$$\chi_{\text{geophysical}}(t) = \frac{0.997}{Cm\Omega}\left[\text{motion} + 0.750 \times \text{matter}\right] \tag{2}$$

$$\chi_{\text{motion}}(t) = \frac{0.997}{Cm\Omega} \times \text{motion} \tag{3}$$

$$\chi_{\text{matter}}(t) = \frac{0.997}{Cm\Omega} \times 0.750 \times \text{matter} \tag{4}$$

where C_m is the principal moment of inertia of the Earth's crust and mantle (taking the Earth's core to be fully decoupled rotationally from the outer planet) and Ω is Earth's mean angular velocity. The factors 0.997 and 0.750 account for the yielding of the solid Earth to surface mass loading and core decoupling. Numerical values for these factors are taken from Dickman (2003) and Gross (2015). The original NCEP and ESMGFZ geophysical excitations are compared in Figure 4.

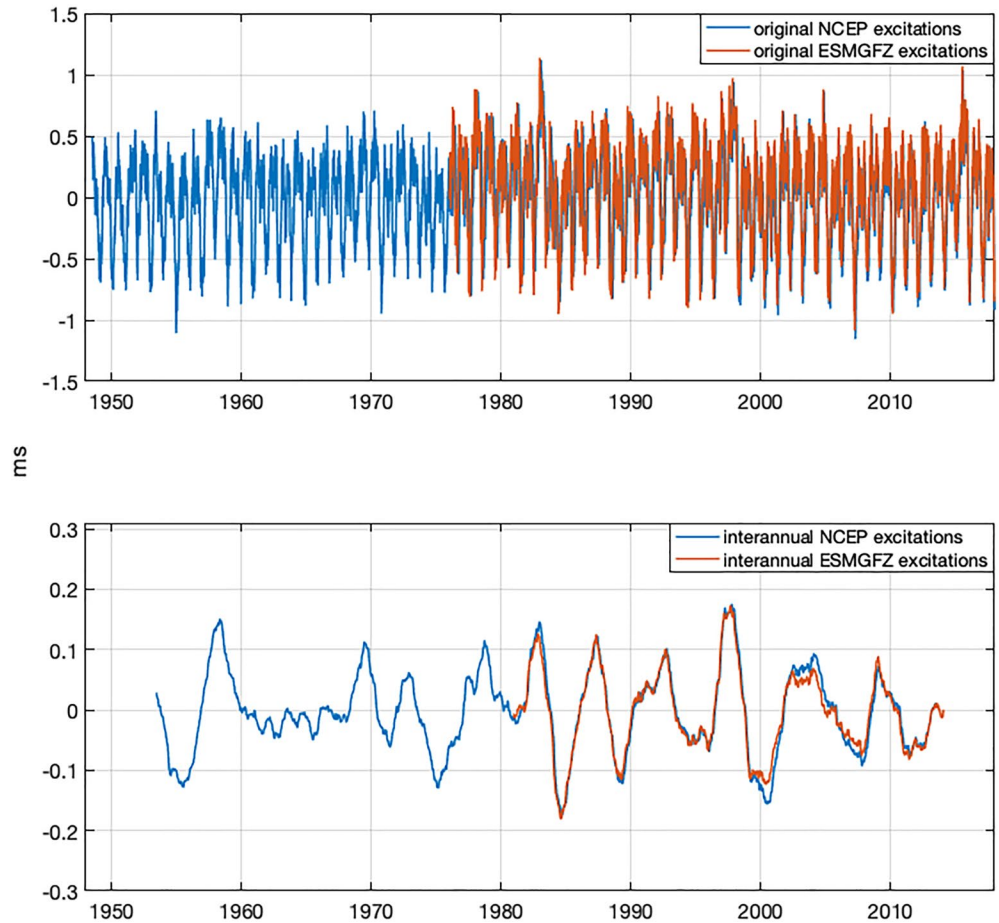

Figure 6. (top panel) Original NCEP/ESMGFZ excitations over the recent period from January 1, 1948 till December 31, 2018 and January 1, 1976 till December 31, 2018. The blue color is the original NCEP excitation series and the red color is the original ESMGFZ excitation series. (bottom panel) Interannual NCEP/ESMGFZ excitations after 8- and 2-year signals removed by sliding window average filtering. The unit of NCEP/ESMGFZ excitations is ms.

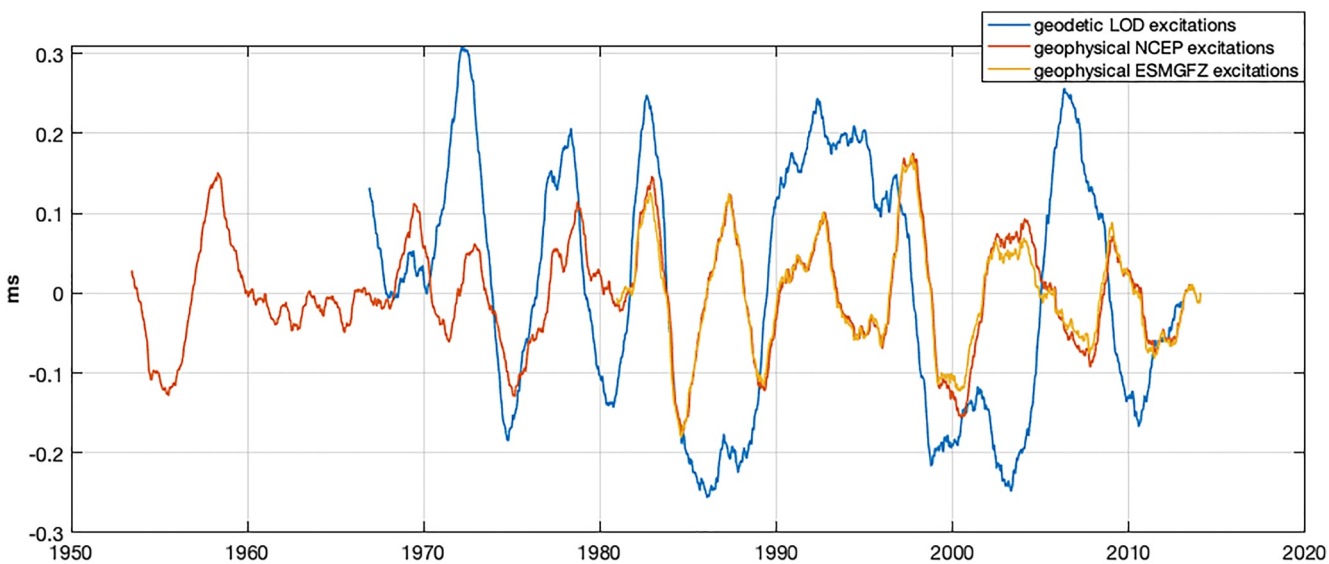

Figure 7. Comparisons between the interannual geodetic LOD excitations from IERS 14C04 and interannual geophysical LOD excitations from NCEP/ESMGFZ.

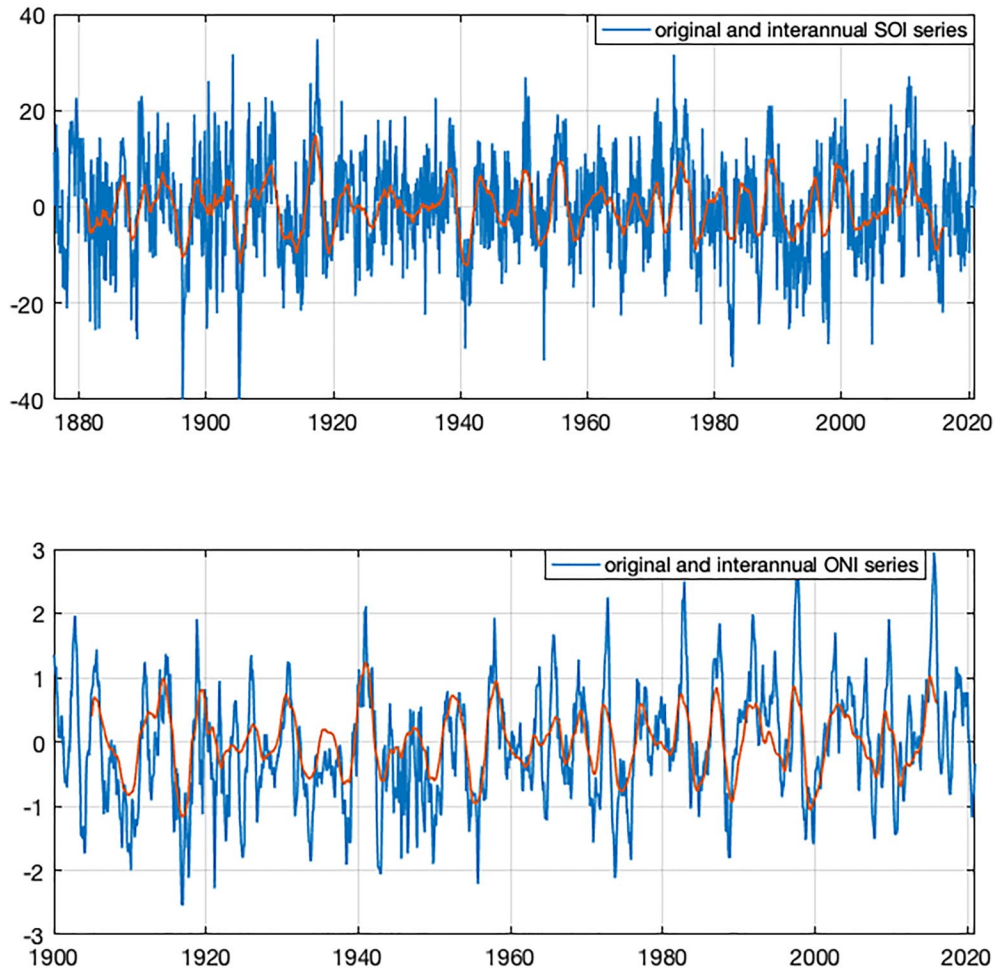

Figure 8. (top panel) Original (blue color) and interannual (red color) SOI series over the recent century from January 1876 till May 2021. (bottom panel) Original (blue color) and interannual (red color) ONI series over the recent century from January 1900 till April 2021.

The SOI/ONI data are sampled every month, the geodetic LOD excitations from IERS 14C04 are sampled every day, and NCEP/ESMGFZ AAMs are sampled every 6 and 3 hr. To match the sampling of SOI/ONI, those IERS 14C04, NCEP, and ESMGFZ data are averaged from daily, 6 and 3 hr to monthly, respectively.

3. Method

For geodetic LOD excitations from IERS 14C04, decadal and longer oscillations are dominant. Eight-year sliding window average filtering is applied first to remove the longer-term (decadal) trends from IERS 14C04 to emphasize the interannual and seasonal variability. Then, 2-year sliding window average filtering is applied again to remove the signals shorter than about 2 years to isolate interannual signals.

As we know, all smoothing methods are unreliable near the ends. The advantage of the sliding window is that the unreliable part is limited strictly to the last bin on each end, not in any of the middle segments. So, in the two lower panels, only data values from 1967 to 2013 (47 years in total) are available.

For NCEP/ESMGFZ AAMs, they are converted to geophysical LOD excitations first, and then 8- and 2-year sliding window average filtering are ap-

Table 4
The Correlation Coefficients Between Interannual ONI, SOI, and NCEP Excitation Series

	ONI/SOI	ONI/NCEP	SOI/NCEP
Correlation coefficients	0.9250	0.8704	0.7372

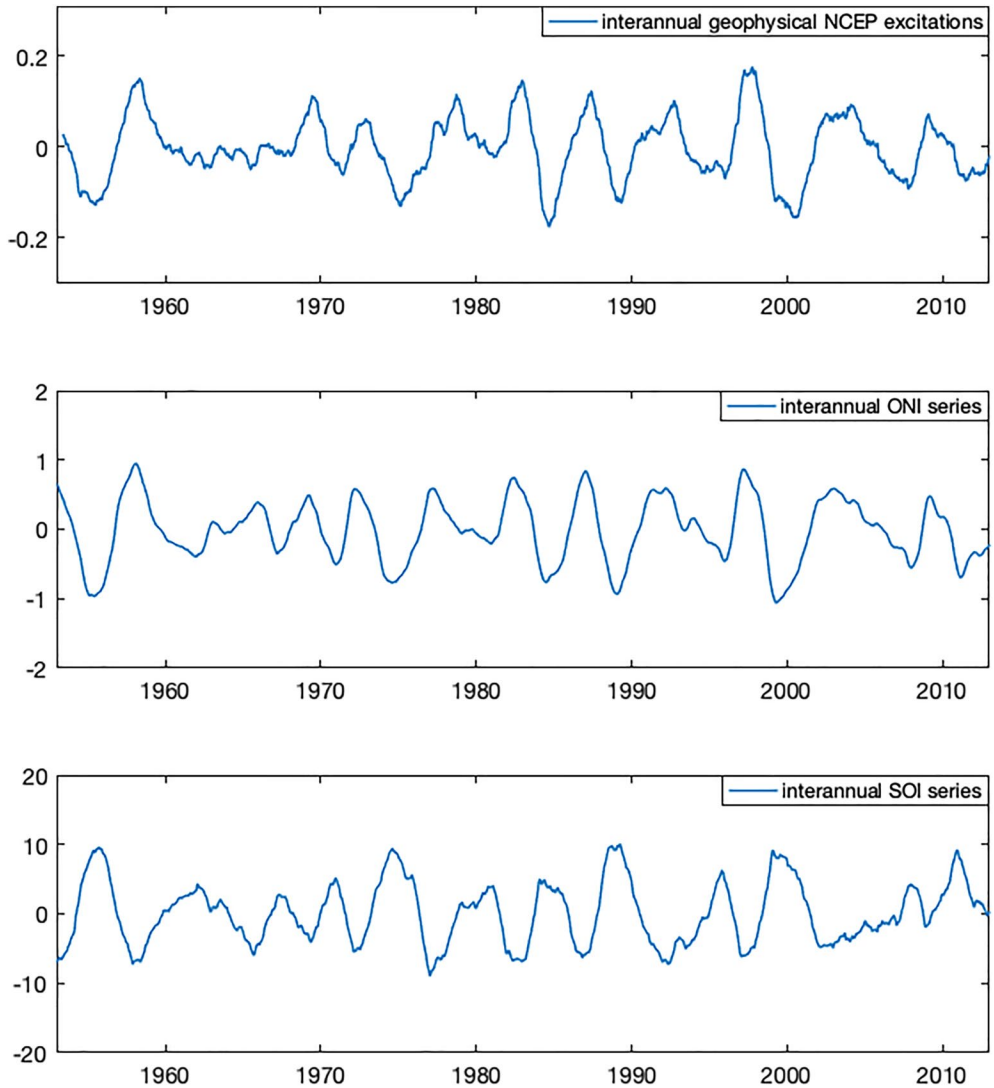

Figure 9. Comparisons between interannual NCEP excitations, ONI, and SOI series.

plied to obtain interannual atmospheric signals. Similarly, for SOI and ONI series, interannual signals can also be obtained after applying 8- and 2-year sliding window average filtering.

4. Results

The original and filtered interannual signals of geodetic LOD excitations are shown in Figure 5.

The original and filtered interannual results of NCEP and ESMGFZ excitations are compared in Figure 6, and the interannual geodetic LOD excitations and geophysical NCEP/ESMGFZ excitations are compared in Figure 7.

From Figure 7 we can see that, there are obvious differences between interannual geodetic and geophysical LOD excitations. We know that atmosphere effects account for most of the LOD variations at yearly and shorter periods, but only accounts for a (limited) part at interannual periods. That is because core–mantle coupling in the deep earth also contributes to interannual LOD excitations. Therefore, comparing the geodetic LOD with that of SOI/ONI is not meaningful thus omitted. Considering the longer time span of NCEP, here we only use NCEP excitations to compare with SOI/ONI series. Due to the data loss during the filtering process, only NCEP excitation series from January 1, 1953 to December 31, 2013 are available (61 years in total). This time span is sufficient for study of interannual and even for decadal signals.

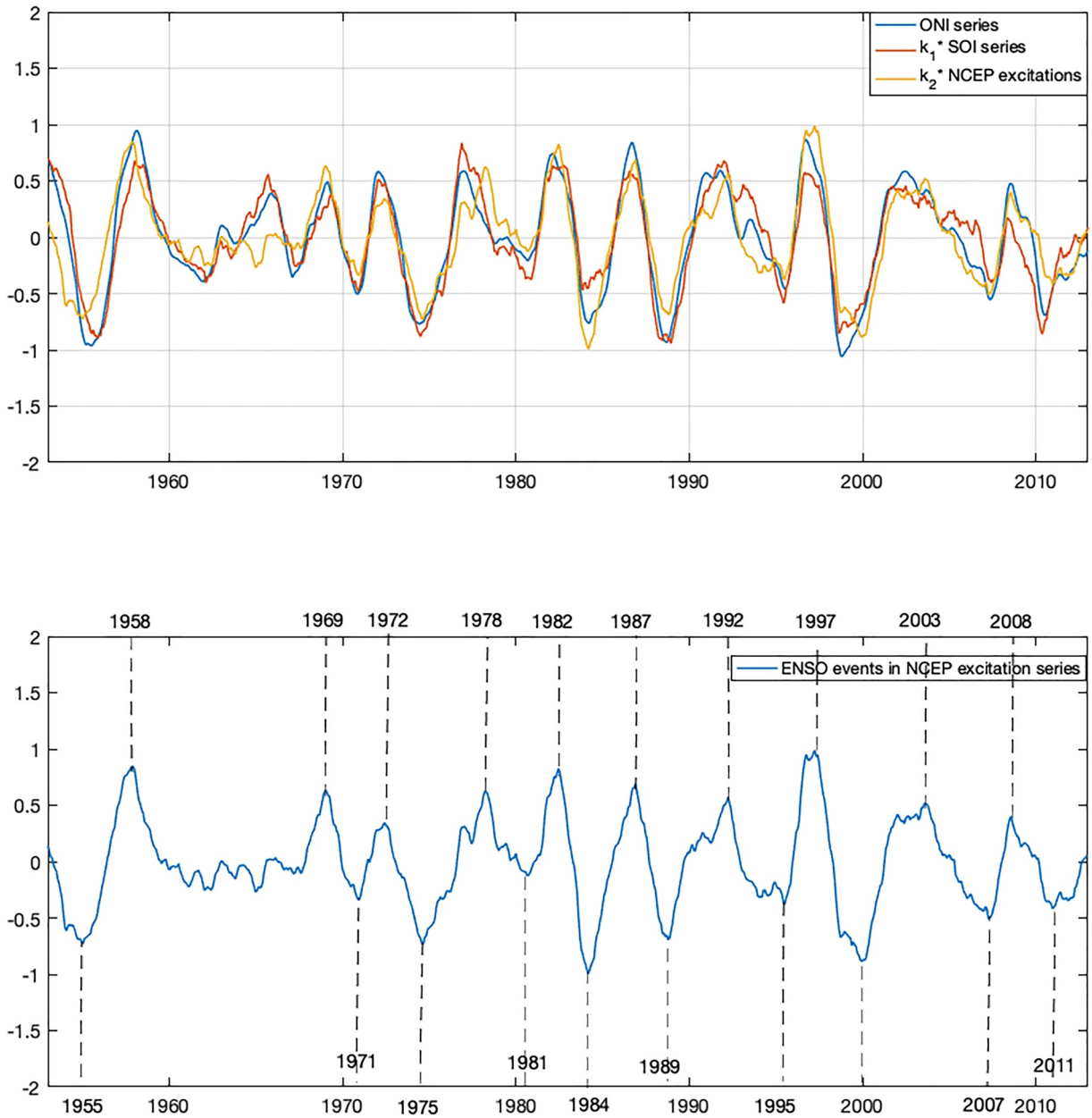

Figure 10. (top panel) Comparisons between the interannual ONI series, $k_1 \times$ SOI series, and $k_2 \times$ NCEP excitation series. (bottom panel) ENSO events in NCEP excitation series.

The original and filtered interannual signals of SOI/ONI series are shown in Figure 8.

First, by calculating the correlation coefficients between interannual ONI, SOI, and NCEP excitation series, we can find that NCEP LOD excitation series are highly correlated with both ONI and SOI series (see Table 4).

Comparing interannual NCEP excitations from bottom panel of Figure 6, interannual SOI/ONI series from Figure 8, we can find that NCEP and ONI series have similar waveforms and trends, while SOI series opposes them in sign. That is because those data sources (SOI series are from air pressure difference, and ONI series are from ocean surface temperature) and evaluation criterions for ENSO events are not the same. The amplitude magnitudes of SOI, ONI, and NCEP time series are significantly different, so we could not compare them with each other directly (see Figure 9).

Here, we derive a gain factor k by minimizing the misfit between ONI series and SOI series, and ONI series and NCEP excitation series through a simple least squares regression (e.g., Chen et al., 2007; Famiglietti et al., 2011; Klees et al., 2007; Swenson & Wahr, 2007):

$$\min = \sum\left(\mathrm{ONI} - k_1 \times \mathrm{SOI}\right)^2 \tag{5}$$

$$\min = \sum\left(\mathrm{ONI} - k_2 \times \mathrm{NCEP}\right)^2 \tag{6}$$

As an illustrative example, we use Equation 5 to derive the gain factor of $k_1 = -0.0934$, which can reduce the variance of $\left|\mathrm{ONI} - \mathrm{SOI}\right|$ from 7.3276 to 0.0095. When the gain factor of $k_2 = 5.7145$ as determined from Equation 6 is applied to NCEP excitations, it becomes evident that NCEP series corresponds quite well with ONI series, for both amplitude magnitudes and waveforms (see Figure 10).

The bottom panel of Figure 10 demonstrates those ENSO events occurred in NCEP excitation series during the period from 1953 to 2013. Referring to the definition by the National Oceanic and Atmospheric Administration (NOAA), if the 3-month sliding average of SST in the Niño 3.4 zone is ≥0.5°C (≤−0.5°C) and lasts for five consecutive months, the event can be defined as an El Niño (La Niña) event. Here, we use a sliding average filtering of 2 years, so it is impossible to strictly compared with 0.5°C, but those peaks/troughs of NCEP or ONI series in Figure 10 can still reflect the fluctuation of an El Niño or La Niña event. For the episodes of 1958, 1969, 1972, 1978, 1982, 1987, 1992, 1997, 2003, and 2008 coincide with El Niño events, and those episodes of 1955, 1971, 1975, 1981, 1984, 1989, 1995, 2000, 2007, and 2011 coincide with La Niña events.

5. Conclusions

In this study, we compared interannual geodetic LOD excitations from IERS 14C04, atmospheric excitations from NCEP/ESMGFZ AAM series, and SOI/ONI series from Australian Bureau of Meteorology. We can make conclusions as follows: (a) according to the high correlations between ONI, SOI, and NCEP series, there are useful information of ENSO events in AAM series; (b) interannual NCEP excitation series correspond quite well with ONI and SOI series after multiplying a gain factor of k, so AAM series also can be used as an index for ENSO events; and (c) based on the reliable modeling and prediction of AAMs, we can search for another way for analyzing and predicting ENSO events.

Data Availability Statement

Data sets for this research are available from the IERS Special Bureau for the Atmosphere and Special Bureau for the Oceans (ftp://hpiers.obspm.fr/iers/eop/eopc04/; http://files.aer.com/aerweb/AAM/aam.ncep.reanalysis.2019), and the GFZ German Research Centre for Geosciences (http://rz-vm115.gfz-potsdam.de:8080/repository/entry/show?entryid=57600abc-2c31-481e-9675-48f488b9304d), respectively.

Acknowledgments
This research is funded by the National Natural Science Foundation of China (grant nos. 42104024 and 41974019), Key Laboratory of Surveying and Mapping Science and Geospatial Information Technology of Ministry of Natural Resources (grant no. 2020-1-2), Hubei Key Laboratory of Marine Geological Resources (grant no. MGR202005), the Basal Research Fund of Chinese Academy of Surveying and Mapping (nos. AR2016 and AR2126), the German Academic Exchange Service (DAAD) Thematic Network Project (grant no. 57421148), and the Opening Fund of Key Laboratory of Geological Survey and Evaluation of Ministry of Education (grant no. GLAB2020ZR12).

References

Allan, R. J., Nicholls, N., Jones, P. D., & Butterworth, I. J. (1991). A further extension of the Tahiti–Darwin SOI, early ENSO events and Darwin pressure. *Journal of Climate*, *4*, 743–749. https://doi.org/10.1175/1520-0442(1991)004<0743:AFEOTT>2.0.CO;2

Altamimi, Z., Rebischung, P., Métivier, L., & Collilieux, X. (2016). ITRF2014: A new release of the International Terrestrial Reference Frame modeling nonlinear station motions. *Journal of Geophysical Research: Solid Earth*, *121*, 6109–6131. https://doi.org/10.1002/2016JB013098

Aoyama, Y., & Naito, I. (2000). Wind contributions to the Earth's angular momentum budgets in seasonal variation. *Journal of Geophysical Research*, *105*(D10), 12417–12431. https://doi.org/10.1029/2000JD900101

Bizouard, C., Lambert, S., Becker, O., & Richard, J. Y. (2017). *Combined solution C04 for earth rotation parameters consistent with International Terrestrial Reference Frame 2014* (technical note). Retrieved from http://hpiers.obspm.fr/iers/eop/eopc04/C04.guide.pdf

Brzeziński, A., Bizouard, C., & Petrov, S. D. (2002). Influence of the atmosphere on Earth rotation: What new can be learned from the recent atmospheric angular momentum estimates? *Surveys in Geophysics*, *23*, 33–69.

Chao, B. F. (1989). Length-of-day variations caused by El Niño–Southern Oscillation and quasi-biennial oscillation. *Science*, *243*(4893), 923–925. https://doi.org/10.1126/science.243.4893.923

Chen, J. L., Wilson, C. R., Famiglietti, J. S., & Rodell, M. (2007). Attenuation effect on seasonal basin-scale water storage changes from GRACE time-variable gravity. *Journal of Geodesy*, *81*, 237–245. https://doi.org/10.1007/s00190-006-0104-2

Davies, C. J., Stegman, D. R., & Dumberry, M. (2014). The strength of gravitational core–mantle coupling. *Geophysical Research Letters*, *41*, 3786–3792. https://doi.org/10.1002/2014GL059836

Deliège, A., & Nicolay, S. (2017). Analysis and indications on long-term forecasting of the Oceanic NIO Index with wavelet-induced components. *Pure and Applied Geophysics*, *174*(4), 1–12.
del Rio, A. R., Gambis, D., & Salstein, D. A. (2000). Interannual signals in length of day and atmospheric angular momentum. *Annales de Geophysique*, *18*, 347–364. https://doi.org/10.1007/s00585-000-0347-9
Dickey, J. O., Marcus, S. L., Hide, R., Eubanks, T. M., & Boggs, D. H. (1994). Angular momentum exchange among the solid earth, atmosphere, and oceans: A case study of the 1982–1983 El Niño event. *Journal of Geophysical Research*, *99*(B12), 23921–23937. https://doi.org/10.1029/94JB01249
Dickman, S. (2003). Evaluation of "effective angular momentum function" formulations with respect to core–mantle coupling. *Journal of Geophysical Research*, *108*(B3), 2150. https://doi.org/10.1029/2001JB001603
Dobslaw, H., & Dill, R. (2018). Predicting Earth orientation changes from global forecasts of atmosphere–hydrosphere dynamics. *Advances in Space Research*, *61*, 1047–1054. https://doi.org/10.1016/j.asr.2017.11.044
Duan, P. S., Liu, G. Y., Hu, X. G., Zhao, J., & Huang, C. L. (2018). Mechanism of the inter-annual oscillation in length of day and its constraint on the electromagnetic coupling at the core–mantle boundary. *Earth and Planetary Science Letters*, *482*, 245–252. https://doi.org/10.1016/j.epsl.2017.11.007
Famiglietti, J. S., Lo, M., Ho, S. L., Bethune, J., Anderson, K. J., Syed, T. H., et al. (2011). Satellites measure recent rates of groundwater depletion in California's central valley. *Geophysical Research Letters*, *38*, L03403. https://doi.org/10.1029/2010GL046442
Feissel, M., & Gavoret, J. (2013). *ENSO-related signals in earth rotation* (pp. 1962–1987). American Geophysical Union (AGU).
Gross, R. S. (2015). Earth rotation variations—Long period. *Physical Geodesy*, *11*, 215–261. https://doi.org/10.1016/b978-0-444-53802-4.00059-2
Hao, D., & Chao, B. F. (2018). A 6-year westward rotary motion in the Earth: Detection and possible MICG coupling mechanism. *Earth and Planetary Science Letters*, *495*, 50–55.
Holme, R., & De Viron, O. (2013). Characterization and implications of intradecadal variations in length of day. *Nature*, *499*, 202–204. https://doi.org/10.1038/nature12282
Kalnay, E., Kanamitsu, M., Kistler, R., Collins, W., Deaven, D., Gandin, L., et al. (1996). The NCEP/NCAR 40-year reanalysis project. *Bulletin of the American Meteorological Society*, *77*(3), 437–471. https://doi.org/10.1175/1520-0477(1996)077<0437:TNYRP>2.0.CO;2
Kantha, L. H., Stewart, J. S., & Desai, S. D. (1998). Long-period lunar fortnightly and monthly ocean tides. *Journal of Geophysical Research*, *103*(C6), 12639–12647. https://doi.org/10.1029/98JC00888
Klees, R., Zapreeva, E. A., Winsemius, H. C., & Savenije, H. H. G. (2007). The bias in GRACE estimates of continental water storage variations. *Hydrology and Earth System Sciences*, *11*, 1227–1241. https://doi.org/10.5194/hess-11-1227-2007
Können, G. P., Jones, P. D., Kaltofen, M. H., & Allan, R. J. (1998). Pre-1866 extensions of the Southern Oscillation Index using early Indonesian and Tahitian meteorological readings. *Journal of Climate*, *11*(9), 2325–2339.
Lambeck, K. (1980). *The Earth's variable rotation: Geophysical causes and consequences*. Cambridge University Press.
Liao, D. C., & Greiner-Mai, H. (1999). A new DELTA LOD series in monthly intervals (1892.0–1997.0) and its comparison with other geophysical results. *Journal of Geodesy*, *73*, 466–477. https://doi.org/10.1007/pl00004002
Liu, L. T., Hsu, T. H., & Grafarend, W. E. (2005). Wavelet coherence analysis of length-of-day variations and El Niño–Southern Oscillation. *Journal of Geodynamics*, *39*, 267–275. https://doi.org/10.1016/j.jog.2004.11.003
Mcphaden, M. J., Zebiak, S. E., & Glantz, M. H. (2006). ENSO as an integrating concept in Earth science. *Science*, *314*(5806), 1740–1745. https://doi.org/10.1126/science.1132588
Munk, W. H., & MacDonald, G. J. (1960). *The rotation of the earth: A geo-physical discussion* (p. 323). Cambridge University Press.
Pavlis, E. C., Sindoni, G., Paolozzi, A., Ciufolini, I., & Gabrielli, A. (2017). El Niño effects on earth rotation parameters from LAGEOS and LARES orbital analysis. *Paper presented at International Conference on Environment and Electrical Engineering (IEEE), Milan, Italy*.
Petit, G., & Luzum, B. (2010). *IERS conventions 2010* (IERS Tech. Note 36). Verlag des Bundesamts für Kartographie und Geodäsie.
Power, S. B., & Kociuba, G. (2011). The impact of global warming on the Southern Oscillation Index. *Climate Dynamics*, *37*(9–10), 1745–1754. https://doi.org/10.1007/s00382-010-0951-7
Rasmusson, E. M., & Wallace, J. M. (1983). Meteorological aspects of the El Niño/Southern Oscillation. *Science*, *222*, 1195–1202. https://doi.org/10.1126/science.222.4629.1195
Roberts, P. H., & Aurnou, J. M. (2012). On the theory of core–mantle coupling. *Geophysical & Astrophysical Fluid Dynamics*, *106*, 157–230. https://doi.org/10.1080/03091929.2011.589028
Ropelewski, C. F., & Halpert, M. S. (1985). North American precipitation and temperature patterns associated with the El Niño/Southern oscillation (ENSO). *Monthly Weather Review*, *114*(12), 2352–2362.
Silva, L., Jackson, L., & Mound, J. (2012). Assessing the importance and expression of the 6 year geomagnetic oscillation. *Journal of Geophysical Research*, *117*, B10101. https://doi.org/10.1029/2012JB009405
Swenson, S., & Wahr, J. (2007). Multi-sensor analysis of water storage variations of the Caspian Sea. *Geophysical Research Letters*, *34*, L16401. https://doi.org/10.1029/2007GL030733
Trenberth, K. E., & Hoar, T. J. (1997). El Niño and climate change. *Geophysical Research Letters*, *24*(23), 3057–3060. https://doi.org/10.1029/97GL03092
Wahr, J., & Bergen, Z. (1986). The effects of mantle anelasticity on nutations, Earth tides, and tidal variations in rotation rate. *Geophysical Journal International*, *87*, 633–668. https://doi.org/10.1111/j.1365-246x.1986.tb06642.x
Wahr, J. M. (1982). The effects of the atmosphere and oceans on the Earth's wobble—I. Theory. *Geophysical Journal International*, *70*, 349–372. https://doi.org/10.1111/j.1365-246x.1982.tb04972.x
Walker, G. T., & Bliss, E. W. (1932). World weather V. *Memories of the Royal Meteorological Society*, *4*(36), 53–84.
Wilson, R. M. (2010). *An examination of the Hadley sea-surface temperature time series for the Nino 3.4 region*. Marshall Space Flight Center, MSFC.
Xin, L., Meshgi, A., & Babovic, V. (2016). Spatio-temporal variation of wet and dry spell characteristics of tropical precipitation in Singapore and its association with ENSO. *International Journal of Climatology*, *36*(15), 4831–4846.
Yoder, C. F., Williams, J. G., & Parke, M. E. (1981). Tidal variations of Earth rotation. *Journal of Geophysical Research*, *86*(B2), 881–891. https://doi.org/10.1029/JB086iB02p00881
Yu, N., Chen, G., Ray, J., Chen, W., & Chao, N. F. (2020). Semi-decadal and decadal signals in atmospheric excitation of length-of-day. *Earth and Space Science*, *7*, e2019EA000976. https://doi.org/10.1029/2019EA000976
Yu, N., Li, J., Ray, J., & Chen, W. (2018). Improved geophysical excitation of length-of-day constrained by Earth orientation parameters and satellite gravimetry products. *Geophysical Journal International*, *214*(3), 1633–1651. https://doi.org/10.1093/gji/ggy204
Yu, N., Ray, J., Li, J., Chen, G., & Chen, W. (2021). Intraseasonal variations in atmospheric and oceanic excitation of length-of-day. *Earth and Space Science*, *8*, e2020EA001563. https://doi.org/10.1029/2020EA001563

Zhang, R., Li, T., Wen, M., & Liu, L. (2015). Role of intraseasonal oscillation in asymmetric impacts of El Niño and La Niña on the rainfall over southern china in boreal winter. *Climate Dynamics*, *45*(3–4), 559–567. https://doi.org/10.1007/s00382-014-2207-4

Zhou, Y. H., Salstein, D. A., & Chen, J. L. (2006). Revised atmospheric excitation function series related to Earth's variable rotation under consideration of surface topography. *Journal of Geophysical Research*, *111*, D12108. https://doi.org/10.1029/2005JD006608